Atomization and Sprays, vol. 16, pp. xx–yy, 2006

VISCOUS POTENTIAL FLOW ANALYSIS OF STRESS-INDUCED CAVITATION IN AN APERTURE FLOW

T. Funada
Department of Digital Engineering, Numazu College of Technology, 3600 Ooka, Numazu, Shizuoka, 410-8501, Japan

J. Wang
Department of Aerospace Engineering and Mechanics, University of Minnesota, 110 Union St. SE, Minneapolis, MN 55455

D. D. Joseph*
Department of Aerospace Engineering and Mechanics, University of Minnesota, 110 Union St. SE, Minneapolis, MN 55455

Original Manuscript Submitted: 10/18/04; Final Draft Received: 6/4/05

*Cavitation in an aperture flow in a flat plate is studied using viscous potential flow. The maximum tension criterion for cavitation used here was proposed by Joseph [*Phy. Rev. *E, vol. 51, pp. 1649–1650, 1995;* J. Fluid Mech., *vol. 366, 367–378, 1998]: "Liquids at atmospheric pressure which cannot withstand tension will cavitate when and where tensile stresses due to motion exceed one atmosphere. A cavity will open in the direction of the maximum tensile stress which is 45° from the plane of shearing in pure shear of a Newtonian fluid." The aperture flow is expressed using a complex potential and the stress is calculated using viscous potential flow. We find that the viscous stress is huge near the tips of the aperture, thus cavitation could be induced.*

INTRODUCTION

It is well known that cavitation may be induced at sharp edges of the inlet of nozzles, such as those used in atomizers. It is at just such edges that the pressure of an inviscid fluid into a nozzle is minimum. At higher pressure drops (larger cavitation number), the liquid in the nozzle may break away from the nozzle wall; the flow then attaches to the sharp edge of the nozzle and is surrounded by atmospheric gas. The term *incipient cavitation* is used to define the situation where cavitation first appears. The term *supercavitation* describes the situation where there is a strong cavitation flow near the nozzle exit, which is very beneficial to atomization. *Total hydraulic flip* describes the situation where the liquid jet completely separates from the nozzle wall. *Hydraulic flip* occurs in a variety of nozzles of different cross sections, provided that the edge at inlet is sharp and not round. The aperture flow in a flat plate considered here (Fig. 1) is a nearly perfect two-dimensional (2D) model of total hydraulic flip. Experiments documenting the transition to hydraulic flip from cavitating have been presented by Bergwerk [1], Soteriou et al. [2], Chaves et al. [3], Laoonual et al. [4], and a few others.

The outstanding property of the hydraulic flip is the disappearance of any sign of the cavitation that was there before the flow detached. To our knowledge, reports of the observations of the disappearance of cavitation are for very low viscosity liquids, such as water and diesel oil. In the analysis of aperture flow that follows, we find cavitation at the sharp edge for all fluids with viscosity larger than zero; but for low-viscosity liquids, it would be very hard to observe.

*Corresponding author e-mail: joseph@aem.umn.edu. This work was supported in part by the NSF under grants from Chemical Transport Systems.

NOMENCLATURE

C_c	contraction coefficient	z'	$= \pi z/2C_c\ell$, nondimensional complex variable
K	$= (p_u - p_d)/(p_d - p_v)$, Cavitation number		
Re	$= \rho\ell U/\mu$, Reynolds number	$\mathbf{u}$	$= (u,v)$ velocity vector
U	uniform velocity at downstream of the edges	$2\mathbf{D}$	rate of strain tensor
		$\mathbf{T}$, T_{ij}	stress tensor
$f(z)$	$= \phi + i\psi$, complex velocity potential	$\mathbf{1}$	unit diagonal matrix
ℓ	half-width of the aperture	α, β, γ	complex functions
p	pressure	δ_{ij}	Kronecker's delta
p_0	total pressure	ϕ	velocity potential
p_a	atmospheric pressure	ψ	stream function
p_d	downstream pressure	ρ	density of fluid
p_u	upstream pressure	λ	$= 2\lvert d^2 f/dz^2\rvert$
p_v	vapor pressure	μ	viscosity
z	$= x + iy$, complex variable	Ω	gravitational potential

Our analysis is based on the theory of stress induced cavitation put forward by Joseph [5], [6][1]; the flow will cavitate at places where the principal tensile stress $T_{11} > -p_v$, where p_v is the vapor pressure. The theory of viscous potential flow allows us to compute these stresses directly and easily from the classical potential flow solution for aperture flow. Liquid samples that are not specially prepared ordinarily do not cavitate at the vapor pressure; various impurities can reduce the cavitation threshold, and degassing followed by massive pressurization can increase the cavitation threshold. It is more realistic to think of p_v

[1]In 2001, we learned that in 1987 Winer and Bair [7] introduced the idea that stress-induced cavitation may enter into the apparent shear thinning of liquid lubricants. They remarked that shear thinning may be the result of a yielding or cavitation process that occurs at a critical value of the tensile stress in the liquid. They further note that for some high-rate viscosity data at atmospheric pressure the principal normal stress may approach quite low values relative to one atmosphere, suggesting the possibility of cavitation or fracture of the material and resulting in a reduced shear stress. In a private communication, Prof. Bair noted that ". . . There was little interest from tribologists, so we dropped it until recently. In the original work we were able to see to the voids by eye using a clear plastic outer cylinder . . ."

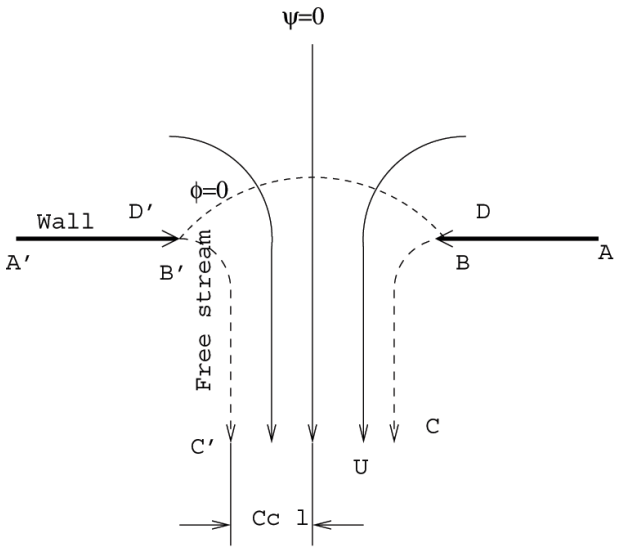

Fig. 1 Flow through an aperture in a flat plate.

as the breaking strength of the liquid, which depends on the history of the liquid sample. Readers may find it convenient to consider the case $p_v = 0$; in this case the sample will fail under tension.

Potential flow is a solution of the Navier-Stokes equations with a gravitational potential Ω and constant viscosity μ

$$\nabla \cdot \mathbf{u} = 0; \ \rho \frac{\partial \mathbf{u}}{\partial t} + \nabla \frac{\rho \mathbf{u} \cdot \mathbf{u}}{2} - \rho \mathbf{u} \times (\nabla \times \mathbf{u}) + \nabla p + \rho \nabla \Omega = \mu \nabla^2 \mathbf{u} \tag{1}$$

For potential flow, $\mathbf{u} = \nabla\phi$, $\nabla \times \nabla\phi = 0$, the equations become

$$\nabla^2 \phi = 0; \ \nabla \left[\rho \frac{\partial \phi}{\partial t} + \frac{\rho \nabla\phi \cdot \nabla\phi}{2} + p + \rho\Omega \right] = 0 \tag{2}$$

Thus, on integration Eq. (2) becomes simply the unsteady Bernoulli's equation albeit that the viscous stresses exist. Namely,

$$\rho \frac{\partial \phi}{\partial t} + \rho \frac{\nabla\phi \cdot \nabla\phi}{2} + p + \rho\Omega = p_0 \tag{3}$$

where p is the isotropic part of the stress tensor

$$\mathbf{T} = -p\mathbf{1} + 2\mu \nabla \otimes \nabla\phi \tag{4}$$

or

$$T_{ij} = -p\delta_{ij} + 2\mu \frac{\partial^2 \phi}{\partial x_i \partial x_j} \tag{5}$$

Since $\nabla^2\phi = 0$

$$-p = \frac{1}{3}(T_{11} + T_{22} + T_{33}) \tag{6}$$

ANALYSIS OF STRESS-INDUCED CAVITATION

The aperture flow in a flat plate is shown in Fig. 1. The magnitude in the resulting jet will reach some uniform value U downstream of the edges. The half-width of the jet is $C_c\ell$, where C_c is the contraction coefficient and ℓ is the half-width of the aperture. The complex potential for this flow is given implicitly by ([8], p. 129)

$$f(z) = \phi + i\psi = -\frac{2C_c \ell U}{\pi} \ln \left\{ \cosh \left[\ln \left(U \frac{dz}{df} \right) \right] \right\} - iC_c \ell U \tag{7}$$

The stress is calculated by

$$\mathbf{T} = -p\mathbf{1} + 2\mu\mathbf{D} \tag{8}$$

The pressure can be calculated using Bernoulli's equation

$$p + \frac{\rho}{2}(u^2 + v^2) = p_d + \frac{\rho}{2}U^2 = p_u \tag{9}$$

where p_u is the upstream pressure and p_d is the downstream pressure at a position where the velocity reaches the uniform velocity U. The velocities are evaluated using from the potential

$$u = \frac{1}{2}\left(\frac{\mathrm{d}f}{\mathrm{d}z} + \frac{\mathrm{d}\bar{f}}{\mathrm{d}\bar{z}}\right), \qquad v = \frac{\mathrm{i}}{2}\left(\frac{\mathrm{d}f}{\mathrm{d}z} - \frac{\mathrm{d}\bar{f}}{\mathrm{d}\bar{z}}\right) \tag{10}$$

It follows that the rate of strain tensor is

$$2\mathbf{D} = \begin{pmatrix} \left(\dfrac{\mathrm{d}^2 f}{\mathrm{d}z^2} + \dfrac{\mathrm{d}^2 \bar{f}}{\mathrm{d}\bar{z}^2}\right) & \mathrm{i}\left(\dfrac{\mathrm{d}^2 f}{\mathrm{d}z^2} - \dfrac{\mathrm{d}^2 \bar{f}}{\mathrm{d}\bar{z}^2}\right) \\ \mathrm{i}\left(\dfrac{\mathrm{d}^2 f}{\mathrm{d}z^2} - \dfrac{\mathrm{d}^2 \bar{f}}{\mathrm{d}\bar{z}^2}\right) & -\left(\dfrac{\mathrm{d}^2 f}{\mathrm{d}z^2} + \dfrac{\mathrm{d}^2 \bar{f}}{\mathrm{d}\bar{z}^2}\right) \end{pmatrix} \tag{11}$$

To use the maximum tension criterion for cavitation, the principal axes coordinates in which $2\mathbf{D}$ is diagonalized need to be found. In the two-dimensional case under consideration here, the diagonalized rate of strain tensor is

$$2\mathbf{D} = \begin{pmatrix} \lambda & 0 \\ 0 & -\lambda \end{pmatrix}, \quad \text{where} \quad \lambda = 2\left|\frac{\mathrm{d}^2 f}{\mathrm{d}z^2}\right| \tag{12}$$

Thus, the maximum tension T_{11} is given by

$$T_{11} = -p + \mu\lambda = -p_u + \frac{\rho}{2}(u^2 + v^2) + \mu\lambda \tag{13}$$

and the cavitation threshold is given by

$$T_{11} = -p_v \tag{14}$$

Combining (13) and (14), we obtain

$$T_{11} + p_v = -p_u + p_v + \frac{\rho}{2}(u^2 + v^2) + \mu\lambda = 0 \tag{15}$$

We use $(\rho/2)U^2$ to render (15) dimensionless

$$\frac{T_{11} + p_v}{\frac{\rho}{2}U^2} = \frac{-p_u + p_v}{p_u - p_d} + \frac{u^2 + v^2}{U^2} + \frac{\mu\lambda}{\frac{\rho}{2}U^2}$$

$$= -\frac{1+K}{K} + \left|\alpha\left(\frac{\phi}{\ell U}, \frac{\psi}{\ell U}\right)\right|^2 + \frac{1}{\mathrm{Re}}\frac{2\pi}{C_c}\left|\beta\left(\frac{\phi}{\ell U}, \frac{\psi}{\ell U}\right)\right| = 0 \tag{16}$$

where the dimensionless parameters are defined as

$$\text{Cavitation number} \quad K = \frac{p_u - p_d}{p_d - p_v} \tag{17}$$

$$\text{Reynolds number} \quad \mathrm{Re} = \frac{\rho \ell U}{\mu} \tag{18}$$

and the complex functions α and β are given by

$$\alpha = \left[e^{\gamma} \pm \sqrt{e^{2\gamma} - 1} \right]^{-1}, \quad \beta = \left[e^{\gamma} \pm \frac{e^{2\gamma}}{\sqrt{e^{2\gamma} - 1}} \right] \alpha^3 \tag{19}$$

with

$$\gamma = -\frac{f + \mathrm{i} C_c \ell U}{2 C_c \ell U} \pi = -\frac{\pi}{2C_c} \frac{\phi}{\ell U} - \frac{\mathrm{i}\pi}{2C_c} \frac{\psi}{\ell U} - \frac{\mathrm{i}\pi}{2} \tag{20}$$

The definition (17) for the cavitation number follows Bergwerk [1] and Soteriou et al. [2] and is somewhat different from the definition by Brennen [9] in which the denominator is the dynamic stagnation pressure.

For a flow with given cavitation number K and Reynolds number (Re), Eq. (16) gives the positions where cavitation inception occurs in terms of $\phi/(\ell U)$ and $\psi/(\ell U)$. The dimensionless description (16) is independent of the vapor pressure or any dimensional parameters entering into the definition of K and Re.

STREAM FUNCTION, POTENTIAL FUNCTION, AND VELOCITY

The complex potential of the flow (7) is implicit and not convenient to use. Therefore, we invert the potential to obtain a function in the form $z = z(f)$. First, we transform the variables as

$$z' = \frac{\pi z}{2C_c \ell}$$

which gives

$$U \frac{\mathrm{d}z}{\mathrm{d}f} = U \frac{\mathrm{d}z}{\mathrm{d}z'} \frac{\mathrm{d}z'}{\mathrm{d}\gamma} \frac{\mathrm{d}\gamma}{\mathrm{d}f} = -\frac{\mathrm{d}z'}{\mathrm{d}\gamma} \tag{21}$$

By virtue of (20) and (21), we have

$$\gamma = \ln \left\{ \cosh \left[\ln \left(-\frac{\mathrm{d}z'}{\mathrm{d}\gamma} \right) \right] \right\}$$

which can be written as

$$e^{\gamma} = -\frac{1}{2} \left[\frac{\mathrm{d}z'}{\mathrm{d}\gamma} + \left(\frac{\mathrm{d}z'}{\mathrm{d}\gamma} \right)^{-1} \right]$$

Thus we obtain

$$\frac{\mathrm{d}z'}{\mathrm{d}\gamma} = -e^{\gamma} - \sqrt{e^{2\gamma} - 1} \tag{22}$$

Integration of (22) gives

$$z' = -e^{\gamma} - \sqrt{e^{2\gamma}-1} + \frac{1}{2\mathrm{i}}\ln\left(\frac{1+\mathrm{i}\sqrt{e^{2\gamma}-1}}{1-\mathrm{i}\sqrt{e^{2\gamma}-1}}\right) - \frac{\pi}{2} \tag{23}$$

We prescribe the value of the complex potential and compute the corresponding position z by (23). The computational results are shown in Fig. 2(a), where the stream and potential functions are plotted in the z plane. The velocity is then obtained using (10) and shown as a vector plot in Fig. 2(b).

Nearly all the flow through the aperture emanates from regions of irrotationality; vorticity generated by no slip at the wall of the aperture is confined to a boundary layer ,and its effects are neglected here. Stress-induced cavitation can arise where the irrotational stresses are very large; but the maximum stress and, hence, the point of inception, is probably at the edge of the aperture where the vorticity is greatest. We will show in the next section that viscous potential flow predicts cavitation at the tip whenever the viscosity is larger than zero. Thereforeo , the effects of vorticity could be important only if they were such as to suppress cavitation at the tip. Even in this case, the fluid could cavitate in the irrotational region outside the boundary layer. We note that the boundary layer is shrinking near the tip of the aperture due to a favorable pressure gradient; the aperture flow is analogous to the flow with suctions on the wall that suppress the boundary layer thickness. Therefore, the boundary layer could be very thin near the tip of the aperture and our theory can be applied to the region near the tip but outside the boundary layer. Our results indicate that cavitation may occur in such regions. The main unsolved question is the extent to which vorticity generated at the boundary of the aperture corrupts the main flow when the Reynolds number is not large.

CAVITATION THRESHOLD

We use water as an example to illustrate the stress-induced cavitation. The vapor pressure of water at 20°C is 2339 Pa, and we assume that the downstream pressure is the atmospheric pressure: $p_d = p_a = 10^5$ Pa. First we calculate the pressure using the Bernoulli's equation (9). The pressure does not depend on the Reynolds number, and we show the pressure distribution for different cavitation numbers in Fig. 3.

The pressure criterion for cavitation is that cavitation occurs when the pressure is lower than the vapor pressure. The minimum pressure in the aperture flow is the downstream pressure and $p_d = 10^5$ Pa > p_v = 2339 Pa. Thus, the pressure criterion predicts no cavitation for the case under consideration. However, we will show that cavitation occurs in the aperture flow according to the tensile stress criterion [5, 6].

We next account for the viscous part of the stress and consider the maximum tension T_{11}. The cavitation criterion is that cavitation occurs when $T_{11} + p_v \geq 0$. T_{11} depends on both the Reynolds number and the cavitation number. We show the contour plot for $(T_{11} + p_v)/(\rho U^2/2)$ with different Re and K in Figs. 4–6.

Although the velocity is continuous everywhere in the aperture flow, its derivative, and therefore the viscous stress, are singular at the sharp edge. Thus at the sharp edge for all fluids with viscosity larger than zero, $T_{11} + p_v$ is always larger than zero and cavitation occurs. In our analysis here, we shall avoid the singular points and calculate the stresses at points very close to the edges. This is partially justified by the fact that, in reality, the edges are not perfectly sharp. As Chaves et al. [3] noted ". . . Microscopic pictures of the nozzle inlet still show however small indentations of the corner, i.e., less than 5 μm[[AU: EDIT OK?]]." (The diameter of the nozzle in their experiments was 0.2 mm or 0.4 mm).

In Figs. 4–6, the curves on which $T_{11} + p_v = 0$ are the thresholds for cavitation. On the side of a $T_{11} + p_v = 0$ curve that is closer to the sharp edge, $T_{11} + p_v > 0$ and cavitation appears; on the other side of the $T_{11} + p_v = 0$ curve, $T_{11} + p_v < 0$ and there is no cavitation.

We single out the threshold curves on which $T_{11} + p_v = 0$ and plot these curves corresponding to different Re and K together, so that we can see clearly the effects of Re and K on the cavitation region. In Figs. 7(a) and 7(b), K is fixed at 1 and 100, respectively; the threshold curves with Re = 1, 2, 5, 10, 20, 50, and 100 are shown. It can be seen that the cavitation region is larger when Re is smaller; when Re is larger, cavitation is confined to a very small region near the edge of the aperture. In Figs. 8(a) and 8(b), Re is fixed at 1 and 10, respectively; the threshold curves with K = 1, 5, 10, 100, and 1000 are shown.

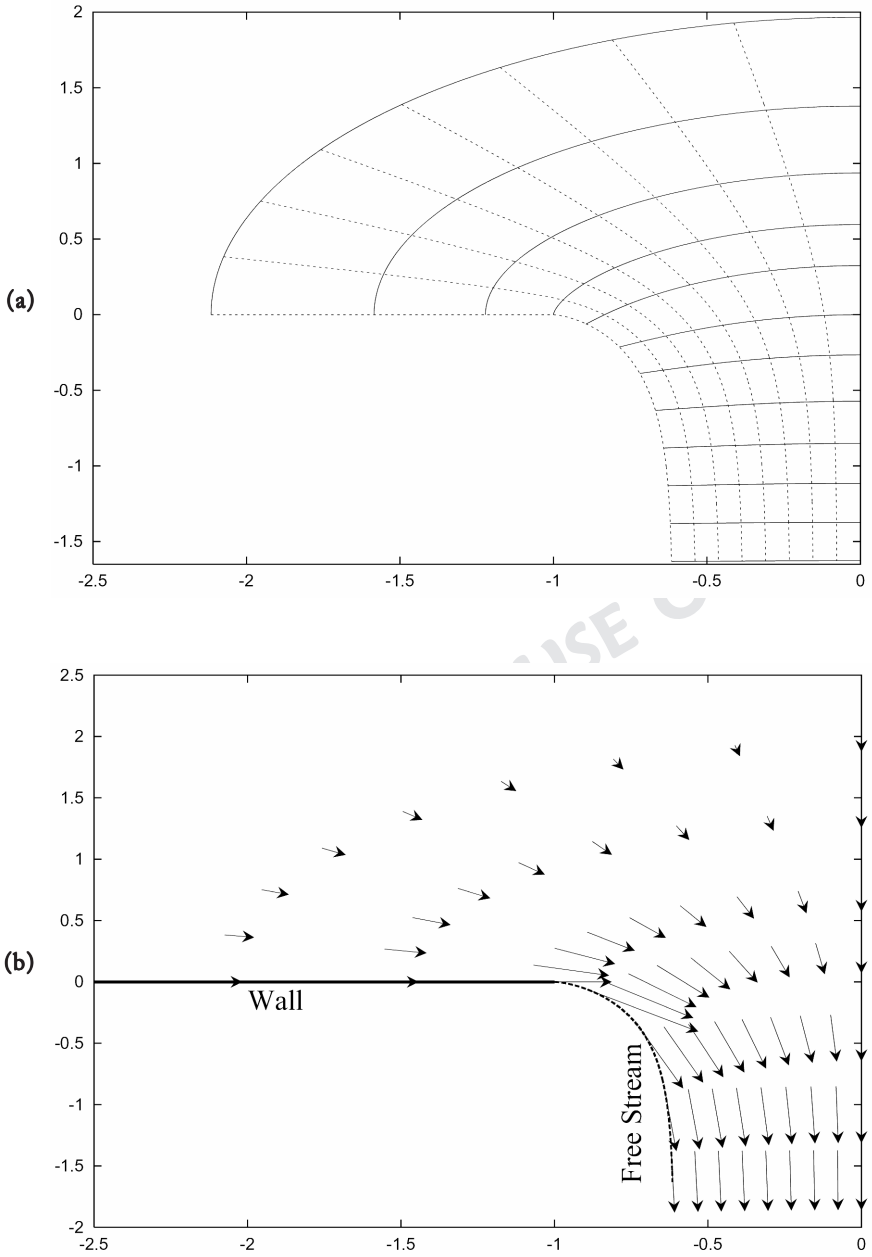

Fig. 2 (a) The stream and potential functions in the z plane. The x and y coordinates are normalized as $(x/\ell, y/\ell)$. The stream and potential functions are in the range $-C_c < \psi/(\ell U) < 0$ and $-0.375 < \phi/(\ell U) < 1.75$, respectively. The contraction coefficient $C_c = \pi/(2 + \pi) = 0.611$, and the edge of the nozzle is at $(x/\ell, y/\ell) = (-1,0)$. (b) The velocity in the z plane. Only half of the flow field is shown due to the symmetry.

One can see that the cavitation region is larger and stretched to far downstream when K is larger. This shows that supercavitation (i.e., cavitation extending to the nozzle exit) can be achieved when K is large. This predicted supercavitation occurs under hydraulic flip condition and is not the same as the supercavitation observed in experiments.

Now we focus on the point ($x/\ell = -1.01$, $y/\ell = 0$), which is upstream to the left sharp edge and very close to it. We can identify values of Re and K that give rise to $T_{11} + p_v = 0$ at this point. These values can be plotted on the Re and K plane, as shown in Fig. 9. On one side of the plotted curve, $T_{11} + p_v > 0$ and cavitation occurs at this point; on the other side, there is no cavitation at this point. Figure 9 shows that small Re and large K favor cavitation. This can be understood readily because small Re leads to large viscous stress and large K leads to small pressure. Both of these effects contribute to a large value of $T_{11} = -p + \mu\lambda$.

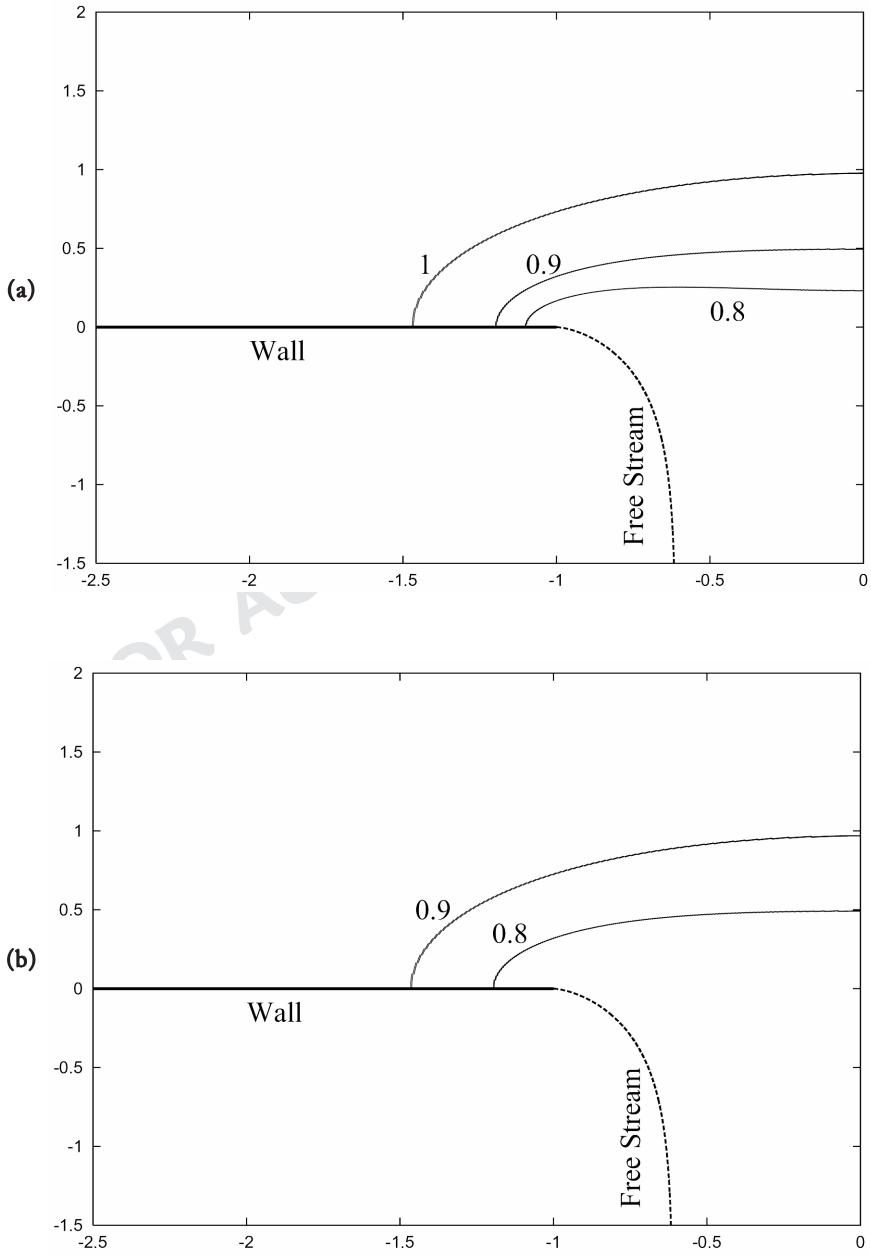

Fig. 3 Contour plot for $(p - p_v)/(\rho U^2/2)$ in the $(x/\ell, y/\ell)$ plane. (a) $K = 10$; (b) $K = 1000$. In the flow field, $p - p_v > 0$ everywhere. Thus there is no cavitation according to the pressure criterion.

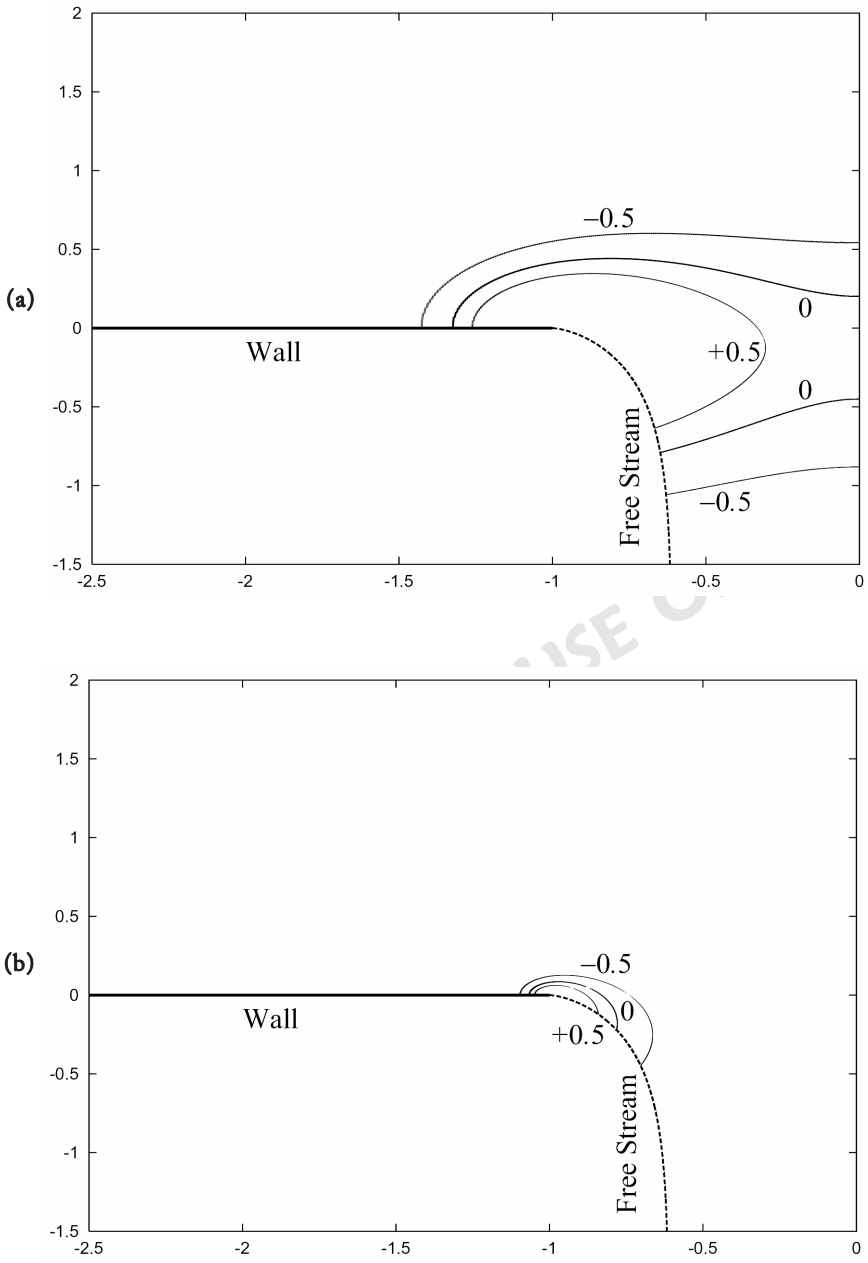

Fig. 4 Contour plot for $(T_{11} + p_v)/(\rho U^2/2)$ in the $(x/\ell, y/\ell)$ plane. (a) $K = 1$ and Re = 1; (b) $K = 1$ and Re = 5. The curve on which $T_{11} + p_v = 0$ is the threshold for cavitation; cavitation occurs inside this curve.

CONCLUSIONS

We use the potential flow through an aperture as a 2D model to study the hydraulic flip observed in injection flows at a nozzle. The pressure in the flow field is computed using Bernoulli's equation, and the viscous stress is evaluated on the potential. The stress tensor is transformed to the principal axes coordinates, and the principal stress T_{11} is obtained. If T_{11} is larger than the negative value of the vapor pressure p_v, the flow will

cavitate. We find that cavitation occurs for all fluids with viscosity larger than zero at the sharp edges of the aperture. The region in which cavitation occurs depends on the Reynolds number Re and the cavitation number K. The cavitation region is larger if Re is smaller and K is larger. The cavitation is confined to very small regions near the edges of the aperture when Re is larger and K is smaller.

Researchers do not observe cavitation in hydraulic flip. The reason may be that the Reynolds numbers in nozzle flows are usually very high (on the order of thousands and tens of thousand). Thus,

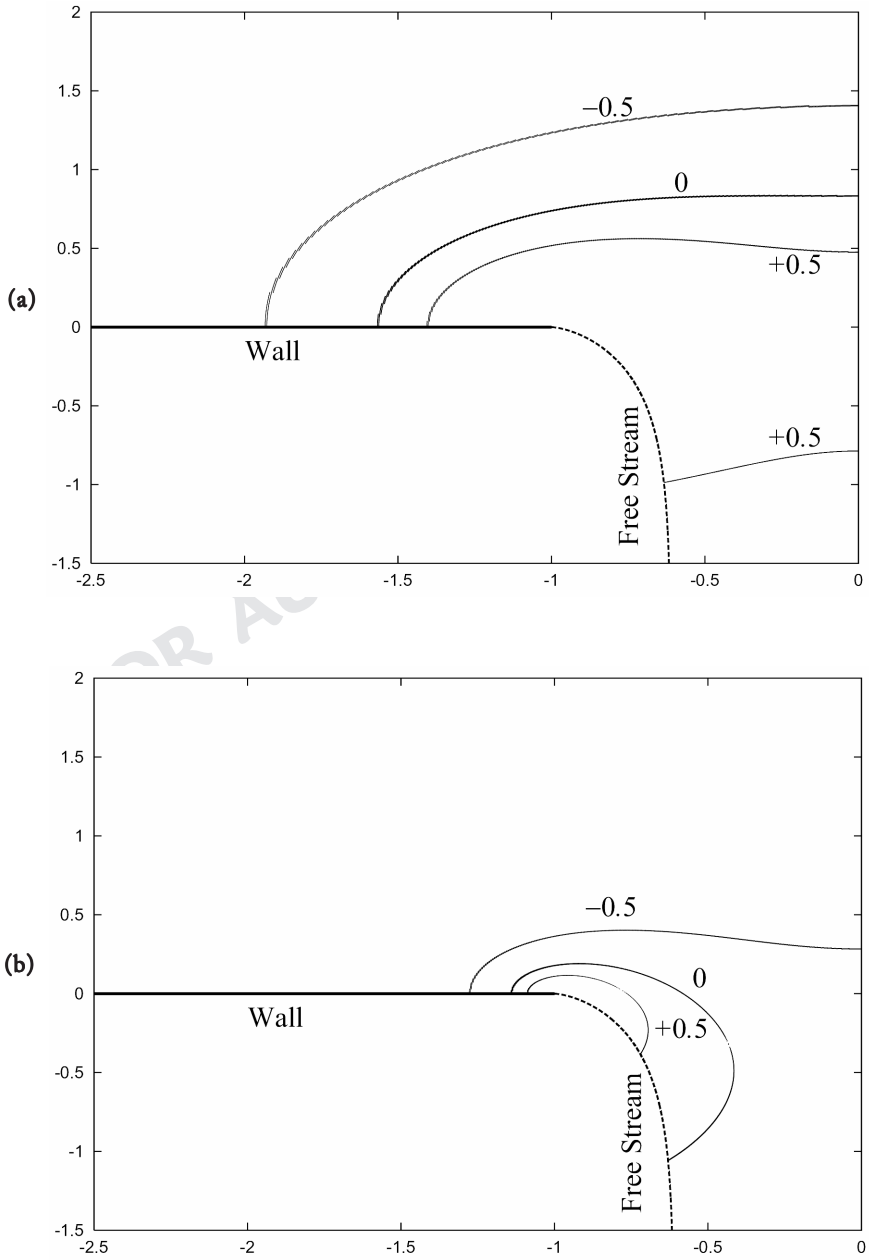

Fig. 5 Contour plot for $(T_{11} + p_v)/(\rho U^2/2)$ in the $(x/\ell, y/\ell)$ plane. (a) $K = 10$ and Re = 1; (b) $K = 10$ and Re = 5. Cavitation occurs inside the curve on which $T_{11} + p_v = 0$.

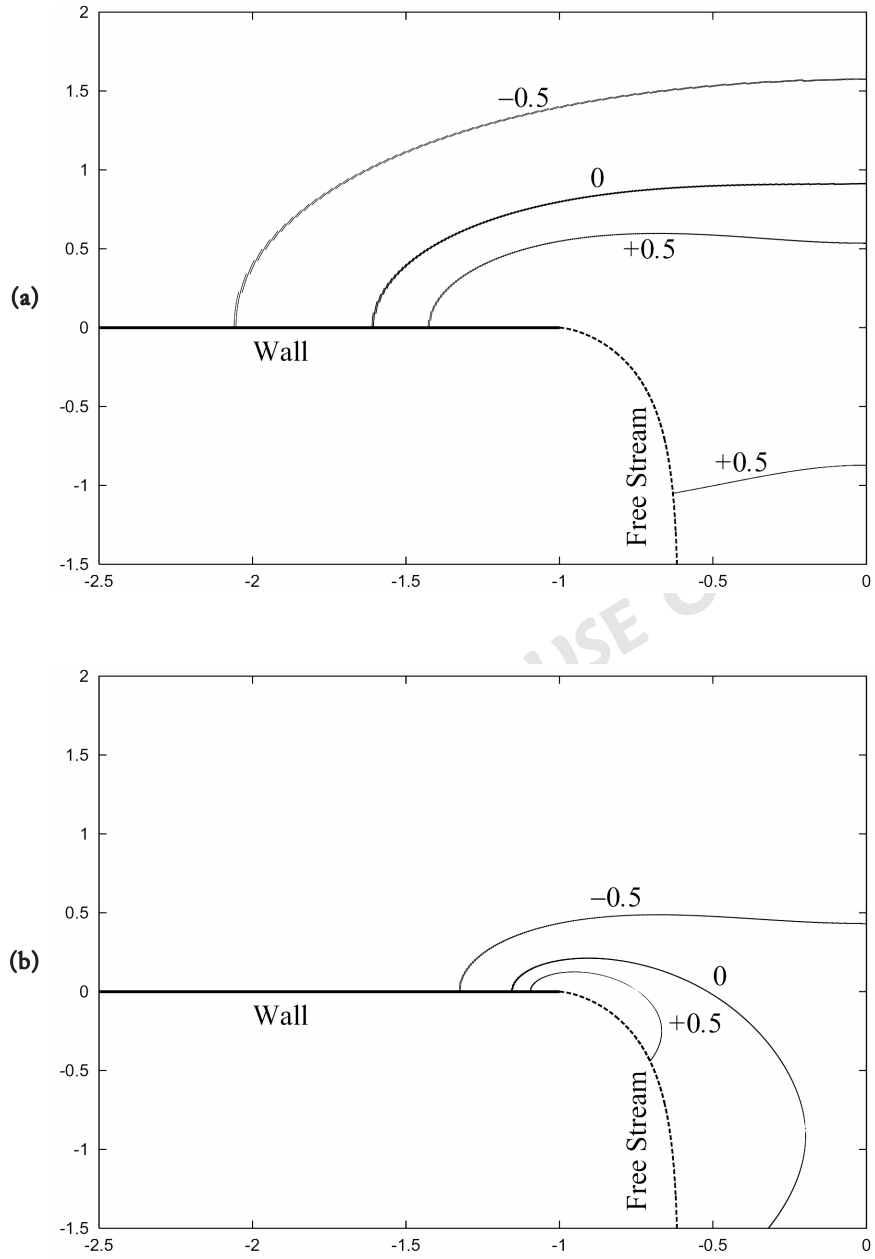

Fig. 6 Contour plot for $(T_{11} + p_v)/(\rho U^2/2)$ in the $(x/\ell, y/\ell)$ plane. (a) $K = 100$ and Re = 1; (b) $K = 100$ and Re = 5. Cavitation occurs inside the curve on which $T_{11} + p_v = 0$.

even if cavitation occurred at the edge of the nozzle, the cavities would collapse quickly outside the small cavitation region (the time for cavities to collapse is on the order of microseconds, according to [3]) and would be very difficult to observe. The effects of liquid viscosity on cavitation are apparently not known; we could not find an evaluation of these effects in the literature. The results obtained here and in Joseph [6] suggest that an increase in viscosity lowers the threshold to stress-induced cavitation.

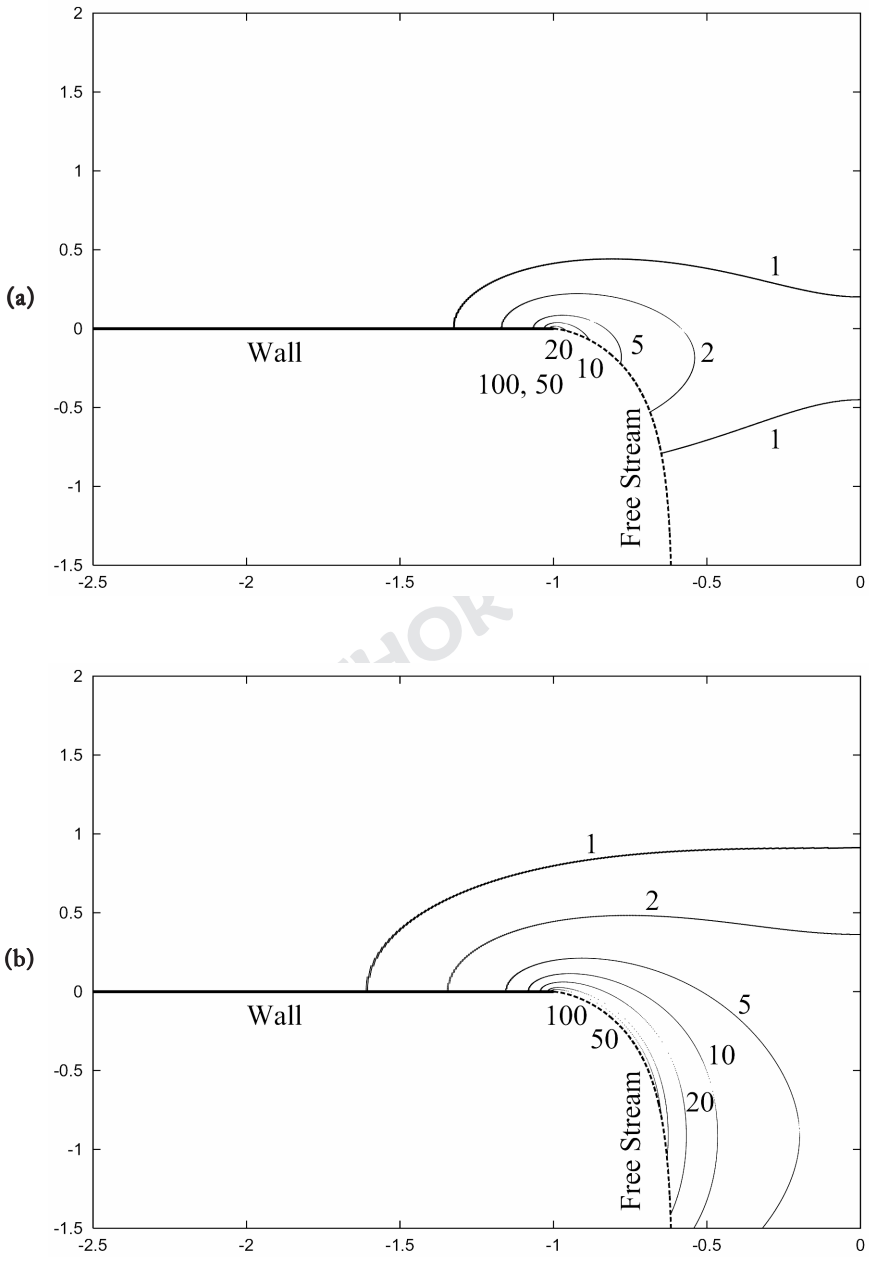

Fig. 7 The cavitation threshold curves on which $T_{11} + p_v = 0$ in different flows with Re = 1, 2, 5, 10, 20, 50, and 100. The cavitation number is fixed at $K = 1$ in (a) and $K = 100$ in (b). Cavitation occurs inside the curve on which $T_{11} + p_v = 0$.

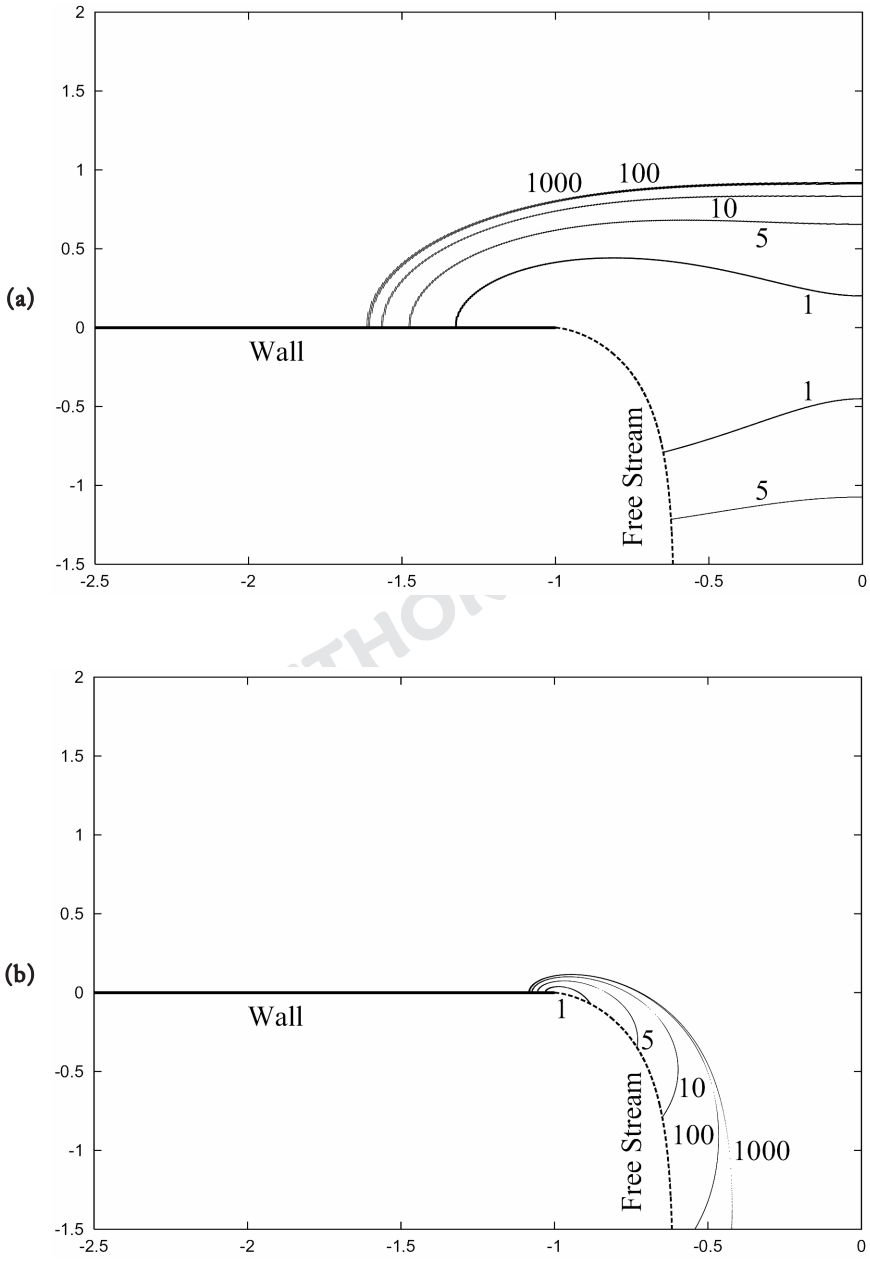

Fig. 8 The cavitation threshold curves on which $T_{11} + p_v = 0$ in different flows with $K = 1$, 5, 10, 100, and 1000. The Reynolds number is fixed at Re = 1 in (a) and Re = 10 in (b). Cavitation occurs inside the curve on which $T_{11} + p_v = 0$.

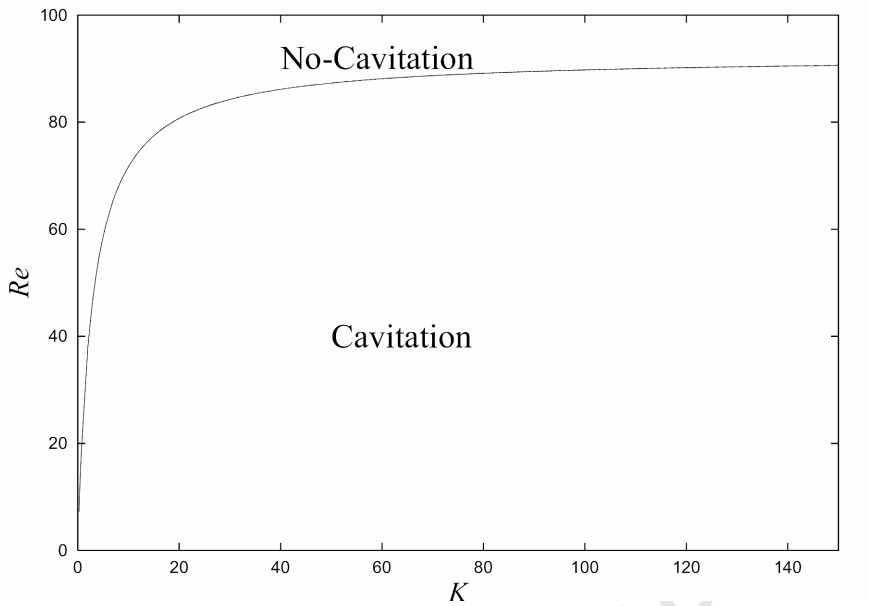

Fig. 9 The curve on which $T_{11} + p_v = 0$ at the point $(x/\ell = -1.01, y/\ell = 0)$ in the Re versus K plane. Below the curve, $T_{11} + p_v > 0$ and cavitation occurs at the point; above the curve, $T_{11} + p_v < 0$ and there is no cavitation at the point.

REFERENCES

1. W. Bergwerk, Flow Patterns in Diesel Nozzle Spray Holes, *Proc. Inst. Mech. Eng.*, vol. 173, pp. 655–660, 1959.
2. C. Soteriou, R. Andrews, and M. Smith, Direct Injection Diesel Sprays and the Effect of Cavitation and Hydraulic Flip on Atomization, SAE Tech. Paper No. 950080, 1995.
3. H. Chaves, M. Knapp, A. Kubitzek, F. Obermeier, and T. Schneider, Experimental Study of Cavitation in the Nozzle Hole of Diesel Injectors using Transparent Nozzles, SAE Tech. Paper No. 950290, 1995.
4. Y. Laoonual, A. J. Yule, and S. J.Walmsley, Internal Fluid Flow and Spray Visualization for a Large Scale Valve Covered Orifice (VCO) Injector Nozzle, *ILASS-Europe 2001*, *Zurich, 2–6 Sept.*, 2001.
5. D. D. Joseph, Cavitation in a Flowing Fluid, *Phy. Rev. E*, vol. 51, pp. 1649–1650, 1995.
6. D. D. Joseph, Cavitation and the State of Stress in a Flowing Liquid, *J. Fluid Mech.*, vol. 366, pp. 367–378, 1998.
7. W. O. Winer and S. E. Bair The INFLUENCE of Ambient Pressure on the Apparent Shear Thinning of Liquid Lubricants: An Overlooked Phenomena, *Proc. of the Institution of Mechanical Engineers-Tribology 50 Years On*, pp. 395–398 Paper No. 190/187, 1987.
8. I. G. Currie, *Fundamental Mechanics of Fluids*, McGraw-Hill, New York, 1974.
9. C. E. Brennen, *Cavitation and Bubble Dynamics*, Oxford University Press, London, 1995.